Preprint typeset in JINST style - HYPER VERSION

Results from the October 2014 CERN test beam of LumiCal[1]

arXiv:1604.00276v1 [physics.ins-det] 1 Apr 2016

O. Borysov[a], V. Ghenescu[b], A. Levy[a], I. Levy[a], S. Lukic[c], J. Moron[d], A.T. Neagu[b], T. Preda[b], O. Rosenblat[a]

On behalf of the FCAL collaboration

[a] *Tel Aviv University, Tel Aviv, Israel*
[b] *ISS, Bucharest, Romania*
[c] *Vinca Institute of Nuclear Sciences, University of Belgrade, Serbia*
[d] *AGH University of Science and Technology, Cracow, Poland*

E-mail: levyaron@post.tau.ac.il

ABSTRACT: A prototype of a luminometer, designed for a future e^+e^- collider detector, was tested in the CERN PS accelerator T9 testbeam. The objective of this test beam was to demonstrate a multi-plane operation, to study the development of the electromagnetic shower and to compare it with MC simulations.

[1] Talk presented at the International Workshop on Future Linear Colliders (LCWS15), Whistler, Canada, 2-6 November 2015.

Contents

1. Introduction **1**

2. Overview of testbeam instrumentation **2**
- 2.1 Mechanical framework 2
- 2.2 Permaglass frames 3
- 2.3 Detector module geometry 4

3. Testbeam area instrumentation **5**

4. Setup and data taking **7**
- 4.1 Telescope alignment and tracking 8

5. Results **10**
- 5.1 Electron-muom separation 10
- 5.2 Signal processing 11
- 5.3 Electromagnetic shower 12

6. Conclusions and outlook **14**

1. Introduction

Two special calorimeters [1] are foreseen in the very forward region of a detector for a future e^+e^- linear collider experiment, the Luminosity Calorimeter (LumiCal) and the Beam Calorimeter (BeamCal). The LumiCal will measure the luminosity with a precision of better than 10^{-3} at 500 GeV centre-of-mass energy and 3×10^{-3} at 1 TeV centre-of-mass energy at the ILC, and with a precision of 10^{-2} at CLIC up to 3 TeV. The BeamCal will perform a bunch-by-bunch estimate of the luminosity and, supplemented by a pair monitor, assist beam tuning when included in a fast feedback system [2].

Both calorimeters extend the detector coverage to low polar angles, important e.g. for new particle searches with a missing energy signature [3]. A sketch of the design is shown in Figure 1 for the ILD detector. The LumiCal is positioned in a circular hole of the end-cap electromagnetic calorimeter ECAL. The BeamCal is placed just in front of the final focus quadrupole. LumiCal covers polar angles between 31 and 77 mrad and BeamCal, between 5 and 40 mrad.

Both calorimeters consist of 3.5 mm-thick tungsten absorber disks, each corresponding to around one radiation length, interspersed with sensor layers. Each sensor layer is segmented radially and azimuthally into pads. The read-out rate is driven by the beam-induced background. Due

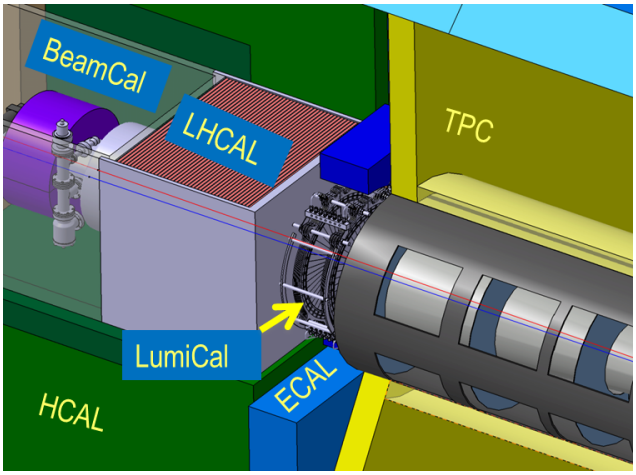

Figure 1: The very forward region of the ILD detector. LumiCal, BeamCal and LHCAL are carried by the support tube for the final focusing quadrupole QD0 and the beam-pipe. TPC denotes the central tracking chamber, ECAL the electromagnetic and HCAL the hadron calorimeter.

to the high occupancy originating from beamstrahlung and two-photon processes, both calorimeters need a fast readout. Front-end (FE) and ADC ASICs are placed at the outer radius of the calorimeters. In addition, the lower polar-angle range of BeamCal is exposed to a large flux of low energy electrons, resulting in depositions up to one MGy for a total integrated luminosity of 500 fb^{-1} at 500 GeV. Hence, radiation-hard sensors are needed. Prototype detector planes assembled with FE- and ADC-ASICs for LumiCal and for BeamCal have been built. In this paper, results of the performance of a prototype of LumiCal, following tests in the CERN PS beam, are reported.

2. Overview of testbeam instrumentation

The performance of fully instrumented LumiCal and BeamCal detector planes was studied in previous testbeam campaigns. The results were fully matching the requirements [4]. The next step in the detector prototype development was to prepare and conduct a testbeam study of a multi-plane structure, performed in October 2014 at the T9 east area of the proton synchrotron (PS) at CERN.

2.1 Mechanical framework

To allow the multiple-plane operation, a sophisticated mechanical structure to meet the demanding geometrical requirements was developed at CERN [5]. The required precision of the shower polar angle reconstruction imposes a precision in the positioning of the sensors of a few tens of micrometers. Since only four detector planes were available, the mechanical structure had to enable modifications in the prototype layout during the testbeam, allowing to measure the longitudinal shower profile. The overall view of the structure of the mechanical frame is presented in Figure 2. The most important component, the layer positioning structure, includes three aluminum combs with 30 slots each, which allow to install the tungsten absorber or active sensor layer with the required precision.

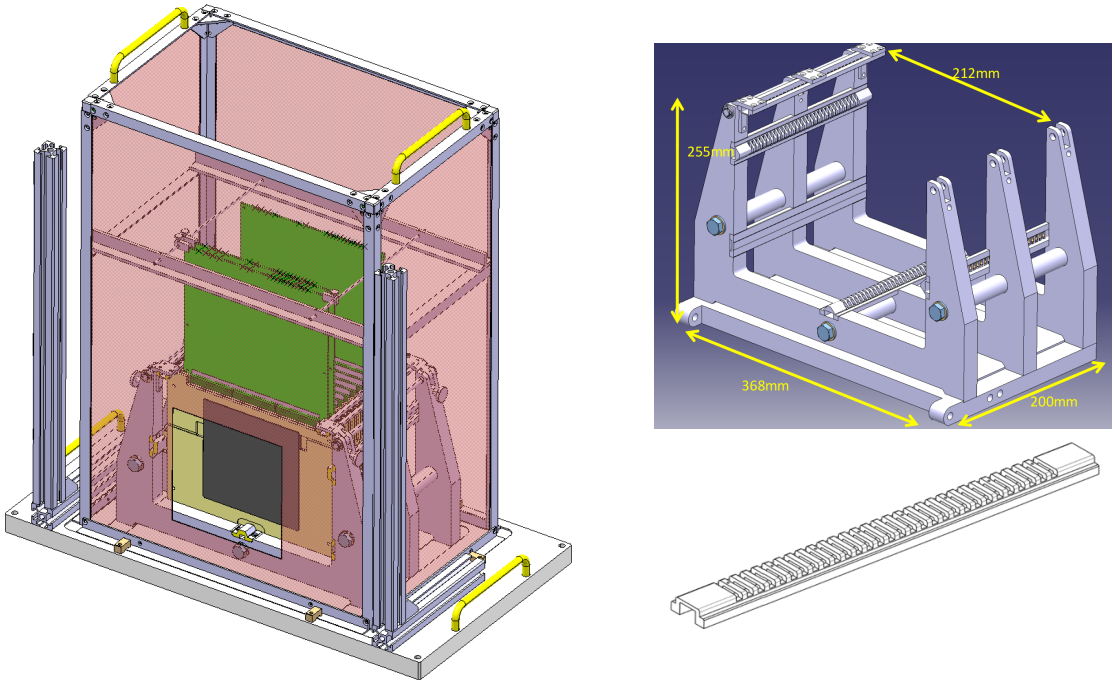

Figure 2: Left-hand side: Scheme of the complete mechanical structure with the tungsten absorbers and readout boards installed. Upper right-hand side: Dimensions of the precision mechanical frame for the positioning of sensor and absorber planes. Lower right-hand side: Detail of the retaining comb jig for positioning of sensor and absorber planes.

2.2 Permaglass frames

The 3.5 mm thick tungsten absorber plates are mounted in permaglass frames, as shown in Figure 3. The light gray inserts located on the left, right (outside) and bottom (inside) sides of the permaglass frames (yellow) contain small bearing balls providing precisely positioned support points for the comb slots. Currently the sensors are mounted onto a 2.5 mm thick PCB[1] serving as the mechanical support and high voltage supply. Therefore, sensor layers are positioned in slots foreseen for tungsten absorber planes to form a stack, as shown in Figure 4 for the first configuration. Different configurations of absorber and sensor planes can be made to measure electromagnetic showers at several positions inside the stack.

The positioning precision of the supporting structure, as well as the tungsten absorber thickness uniformity, were extensively tested [5]. The maximum differences between the theoretical and measured absorber plane positions do not exceed the required ± 50 μm precision[2]. A function test of the fully assembled stack was performed before installation in the testbeam and the full detector prototype functionality was confirmed.

[1] this thickness will be reduced in the future to be less than 1 mm using a sophisticated connectivity scheme under development. Then sensor planes will be positioned in the 1 mm gap between absorber planes.

[2] This requirement will become relevant when thin sensor planed will be used in the future.

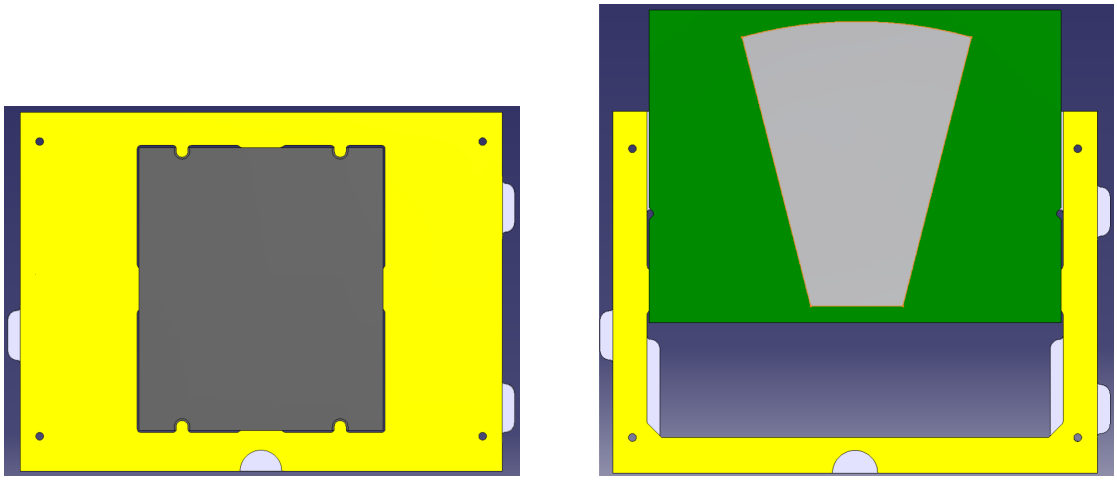

Figure 3: Detector layers supporting frames. Left-hand side: tungsten absorber (gray) in a permaglass frame (yellow). Right-hand side: sensor (gray) PCB (green) partially retracted from a permaglass frame (yellow).

2.3 Detector module geometry

For 5 GeV electrons from the PS accelerator beam the expected maximum of the shower is located around the 6th absorber layer. In order to measure the full shower development, data should be taken with at least the first 10 layers instrumented. Since only four readout boards are available, this condition could be met only with at least three absorber layers placed between each active sensor layer. However, this leads to a rather small number of measurements which could result in large uncertainties in the shower shape. Since the mechanical support structure enables relatively simple detector geometry changes, a different approach was applied. Three different detector configurations were used, with the active sensor layers always separated by two absorber layers. By adding additional absorber layers upstream the detector, the sensor layers were effectively moved downstream in the shower. The first stack configuration is shown in Figure 4. A summary of all configurations used is given in Table 1. The single absorber layer after the last silicon sensor was added in order to simulate the particles backscattering as it takes place in the target detector. The

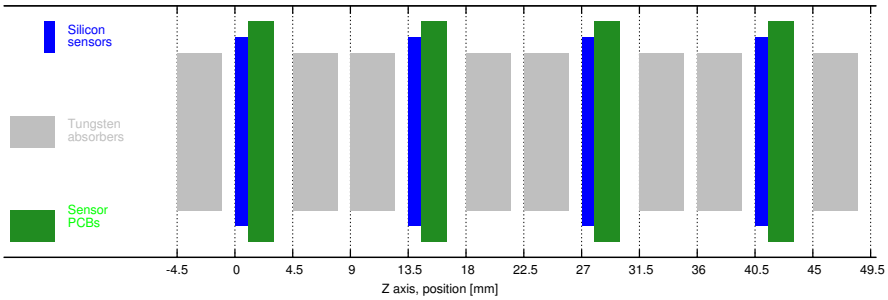

Figure 4: Geometry of the first configuration of the LumiCal detector prototype with active sensor layers located in place of tungsten absorbers. The Y axis (perpendicular to Z) is not to scale.

shower can be therefore sampled up to the 10th layer with a shower sampling resolution of one radiation length. Since the positions of sensors S1–S3 in the first configuration are replicated by the S0–S2 in the second one, the measurement results for the corresponding sensors from both configurations should be almost identical, being a lever arm to control response variation in the measurement. The data can be combined in order to imitate the detector prototype comprising nine active sensor layers. Due to a malfunctioning of the FPGA on the readout board of S3 in the third

	Radiation lengths in number of absorber layers									
Configuration	1	2	3	4	5	6	7	8	9	10
1	S0		S1		S2		S3			
2			S0		S1		S2		S3	
3				S0		S1		S2		S3

Table 1: Positions of active sensor layers in three configurations expressed in number of absorber layers (i.e. radiation lengths in absorber X_0) in front of the sensor layer. S0–S3 stands for Sensor 0 – Sensor 3.

configuration, only eight positions are used in the analysis.

3. Testbeam area instrumentation

The PS accelerator provides a primary proton beam with momentum of 24 GeV/c. Since the beam is shared between different testbeam instrumentations and the LHC beam delivery system, the primary beam for the T9 area is provided in 400 ms long spills with a typical time separation of 33.6 s between them. The primary beam is converted using several targets and for the present testbeam it provided a secondary beam with muons, pions, hadrons and electrons with momenta in the range of 1–15 GeV/c. A narrow band of particle momenta centered at 5 GeV was selected using a dipole magnetic field and a set of collimators. The simplified overall view of the PS east area testbeam facility is presented in Figure 5.

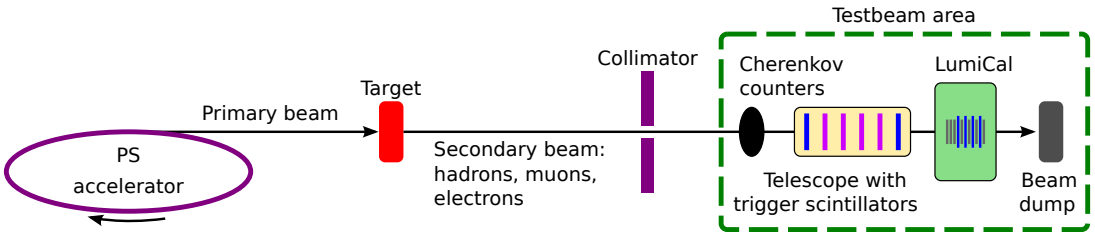

Figure 5: Overall, simplified view (not to scale) of the testbeam instrumentation.

A photograph showing the details of the testbeam area instrumentation is presented in Figure 6. The schematic diagram of the instrumentation geometry is shown in Figure 7. Since the secondary beam consists of a mix of various particles, the Cherenkov counters were used to discriminate the electrons or/and muons. The gas Cherenkov counters allow particle identification as well as the energy discrimination by changing the HV of the photomultiplier and the pressure of the CO_2. For an electron energy of 5 GeV, the gas pressure was set to 53 kPa with the HV set to 1900 V and 1950 V for the first and second Cherenkov counter, respectively. To reconstruct

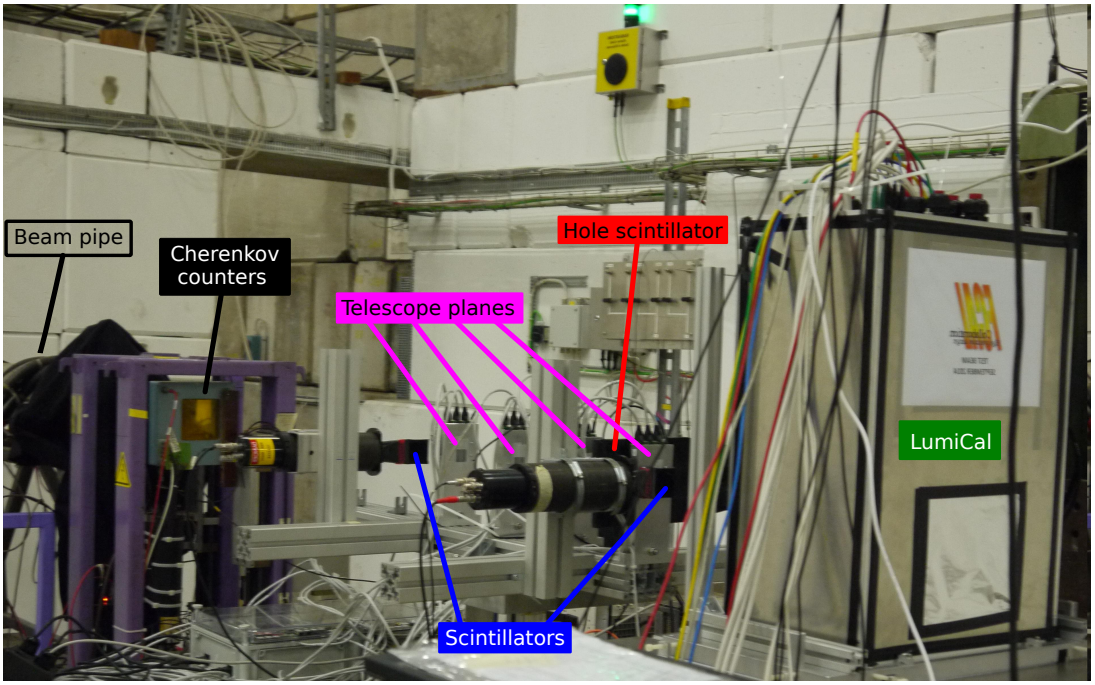

Figure 6: Overall photograph of the testbeam area instrumentation.

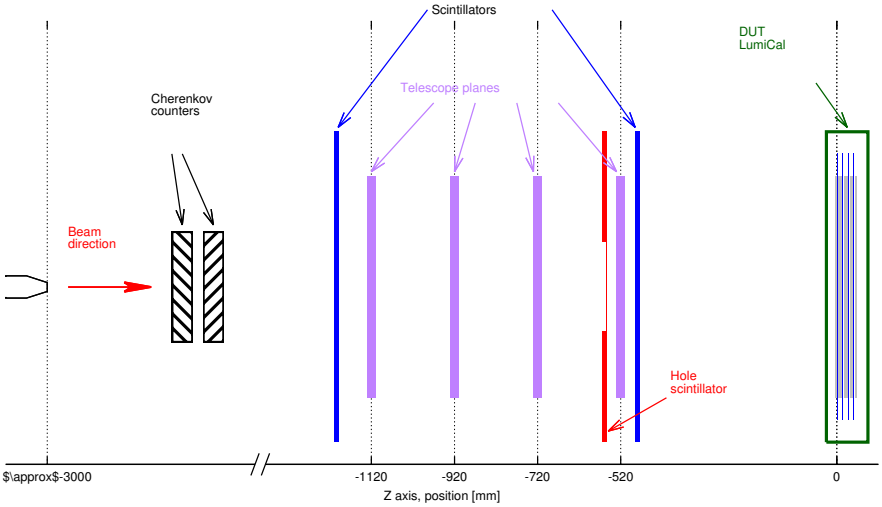

Figure 7: Testbeam area instrumentation geometry. Not in scale.

the trajectories of beam particles a multilayer tracking detector, the so-called telescope, developed by the Aarhus University, was used. The telescope utilizes the MIMOSA-26 chips, a monolithic active pixel sensor with fast binary readout [6]. One MIMOSA-26 chip comprises 1152 $\times$ 576 pixels with 18.4 μm pitch, resulting in an active area of 21.2 $\times$ 10.6 mm^2. The binary readout accepts the pixel signals exceeding a preset discrimination level. The pixel matrix is read continuously providing a complete frame every 115.2 μs. The data are gathered, triggered and stored by a custom DAQ system, based on the National Instrument PXI crate, developed by the Aarhus

University in collaboration with the Strasbourg University. Four telescope planes, each comprising one MIMOSA-26 chip, were set upstream of the stack as shown in Figure 7. Three scintillation counters were used to provide a trigger for particles traversing the active part of the telescope sensors and the region of the sensors in the stack being read out. Two 5×5 cm^2 scintillators tiles were placed upstream and downstream of the telescope (marked in blue in Figure 7) and one (marked in red), with a 9 mm diameter circular hole, was placed just before the last telescope plane. Compact photomultipliers were attached to the scintillators providing electrical pulses. In order to ensure that triggers are only generated by beam particles in the sensitive area of the telescope, the signal from the hole scintillator was set in anti-coincidence. The trigger signal was combined with the Cherenkov counters response, as shown in Figure 8, to create a trigger for electrons. A fraction

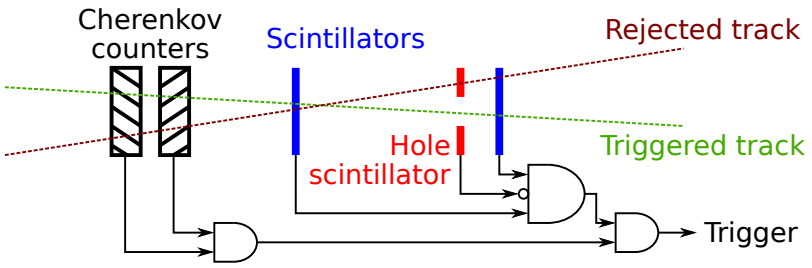

Figure 8: Scheme of the trigger system (see text).

of particles passing through the active area of the anti-coincidence scintilator are registered due to partial inefficiency of the scintilator. An exemplary track of such particle is shown in Figure 8 as a dark-red line, labeled as a rejected track.

The main limitation in the data statistics is the split into 400 ms long spills, containing typically 10^3–10^4 particles. Taking into account the spill repetition frequency, slightly below 2 per minute ($\approx$0.03 Hz), and the electron fraction of about 5 %, a rate of 1.5–15 electrons per second was expected. In addition, the DAQ applies a veto mechanism rejecting triggers during the event data packaging. As a result, some of the electron triggers generated during the 400-ms long spill will be rejected, reducing the average event rate. Since the MIMOSA-26 chip provides a continuous readout, a high particle intensity during short spills can produce multiple track events, to be considered in the data analysis.

4. Setup and data taking

There were two independent DAQ computers for the telescope and for LumiCal. In order to monitor and distribute the trigger signal correctly, a trigger logic unit (TLU) [7] was used. The TLU receives the trigger signal and generates an integer TLU number, counting the number of triggers received. The TLU then passes on the trigger signal and the TLU number to the telescope and the stack, respectively. In order to coordinate between the TLU number and the telescope frame number a dedicated auxiliary (AUX) unit was used, saving these two numbers for the same event. Figure 9 displays the connections and the flow of information in the system.

In each of the sensor planes, the connected pads were pads 51-64 of sector L1 and 47-64 of sector R1, as shown in Figure 10. Upon the arrival of a trigger, the 32 channels were recorded with

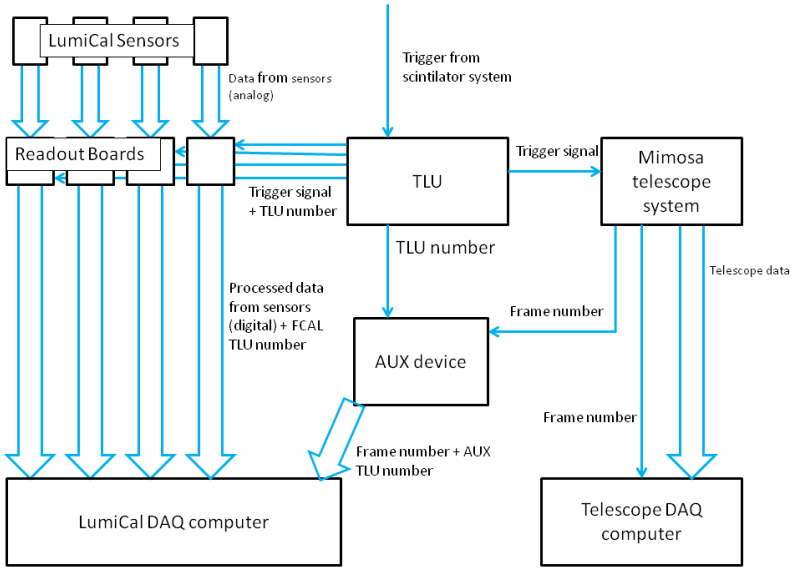

Figure 9: A schematic of the connections and the path of the signal in the system. Data is symbolized by a thick arrow, while simple bit information (e.g. the trigger signal) is symbolized by a thin arrow.

32 samplings in the ADC in steps of 50 ns, resulting in a total read time of 1.6 μs. For each trigger, the TLU number from the LumiCal DAQ, the TLU number from the AUX and the telescope frame number from the AUX were stored for the purpose of synchronization between the stack and the telescope data.

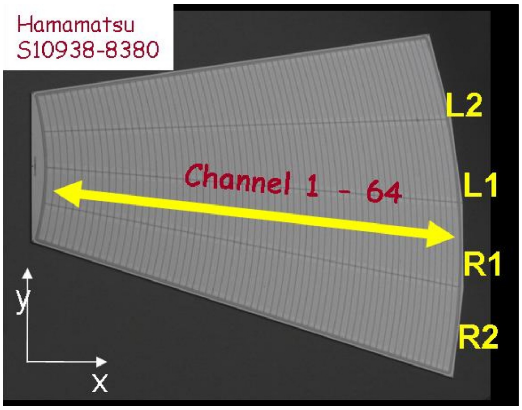

Figure 10: A prototype silicon sensor for LumiCal.

4.1 Telescope alignment and tracking

Since for the given trigger and beam structure a single particle track per event in average was estimated, the expected particle hit count per event per telescope plane is around one. However, the noise hits contribution is quite high and dominates over hits generated by the beam particles, especially for the fourth telescope plane.

As the positions of the telescope planes were only roughly set by the telescope mechanical support structure, an alignment was required to define and correct for the testbeam telescope planes mutual positions. This was done using the standard procedure implemented in TAF [8].

The results of the procedure described above can be seen in the hit-maps for the reconstructed tracks, shown in Figure 11. The beam profile can be clearly seen for the reconstructed tracks.

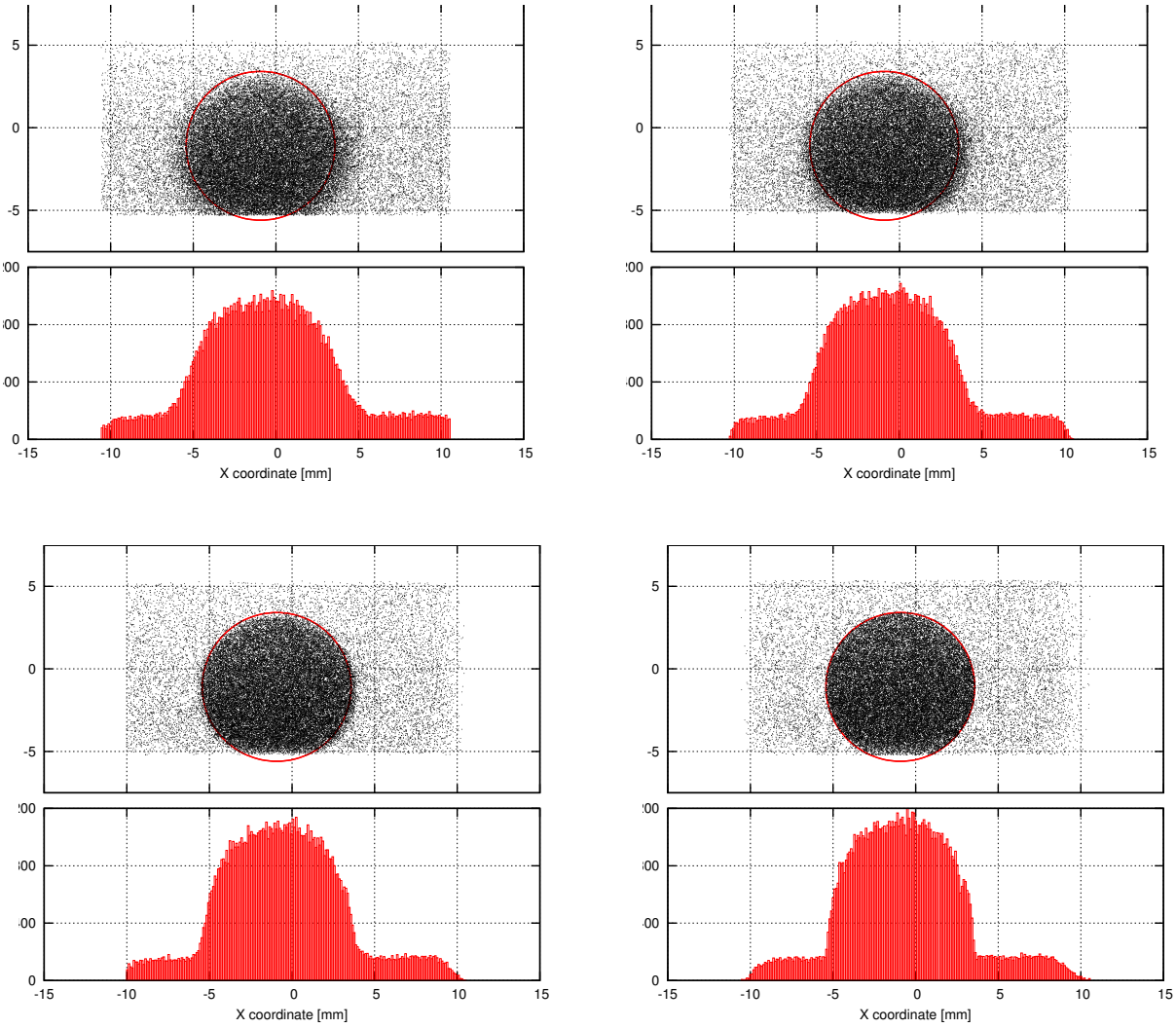

Figure 11: Maps of telescope hits assigned to a track(after data processing, top part of figure) together with the projection on the X axis (bottom part of figure). The red circle represents the hole in the anti-coincidence scintillator. The four figures show the hits in each of the four planes, respectively.

In particular, the distribution for the last telescope plane remains, as expected from the geometry, in very good agreement with the hole in the anti-coincidence scintillator. The number of tracks passing the hole was estimated to be above 95 %, in good agreement with the expected efficiency of the trigger scintillators for the detection of 5 GeV electrons.

5. Results

Each channel of the front-end ASIC comprised a charge-sensitive amplifier, a pole-zero cancellation circuit (PZC), and a first order CR-RC shaper. It was designed to work in two modes: the physics mode and the calibration mode. In the physics mode (low gain), the detector is sensitive to electromagnetic showers resulting in high energy deposition and the front-end electronics processes signals up to almost 10 pC per channel. In the calibration mode (high gain), it detects signals from relativistic muons, considered as approximate Minimum Ionizing Particles (MIPs), to be used for calibration and alignment. To match the ILC timing, the shaper peaking time, T_{peak}, was set to about 60 ns. The prototype ASIC, containing 8 front-end channels, was designed and fabricated in 0.35 μm four-metal two-poly CMOS technology.

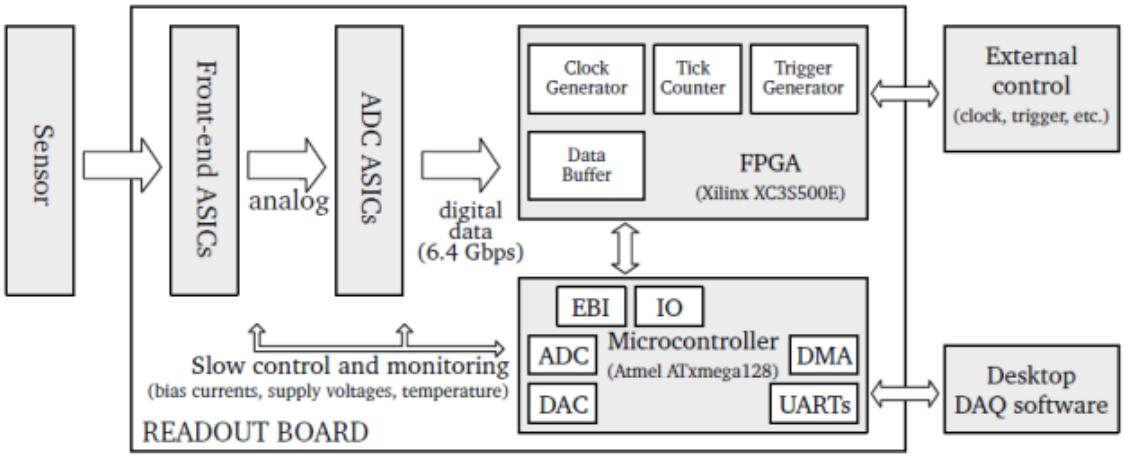

Figure 12: Block diagram of the reaout chain.

To analyze the testbeam data and to perform pile-up studies, a sufficiently high ADC sampling-rate and very high internal-data throughput between the ADC and the FPGA-based back-end electronics was assured. The signals from 32 channels were sampled with a 20 MS/s rate, and digitised with a 10-bit resolution, resulting in a peak data rate of about 6.4 Gb/s. The complete module had 4 multichannels chips with 8 channels each. The read-out chain, shown in Figure 12, contained the Si-sensor, kapton fan-out, front-end electronic and multichannel 10-bit pipeline ADC ASIC. The ASIC is controlled by FPGA-based data concentrator. A photograph of an assembled detector module is shown in Fig. 13.

Testbeam data were analyzed offline using a dedicated software.

5.1 Electron-muom separation

The triggered beam particles contained a few percent of muons. Before extracting the energy deposition, it was necessary to separate the muons from electrons. Figure 14 shows the raw energy spectrum (in ADC counts) for a beam containing electrons and muons, obtained as the sum of all 128 channels in the stack for one event. The high narrow distribution peaking around 120 countsis

Figure 13: Photograph of a LumiCal readout module with a sensor.

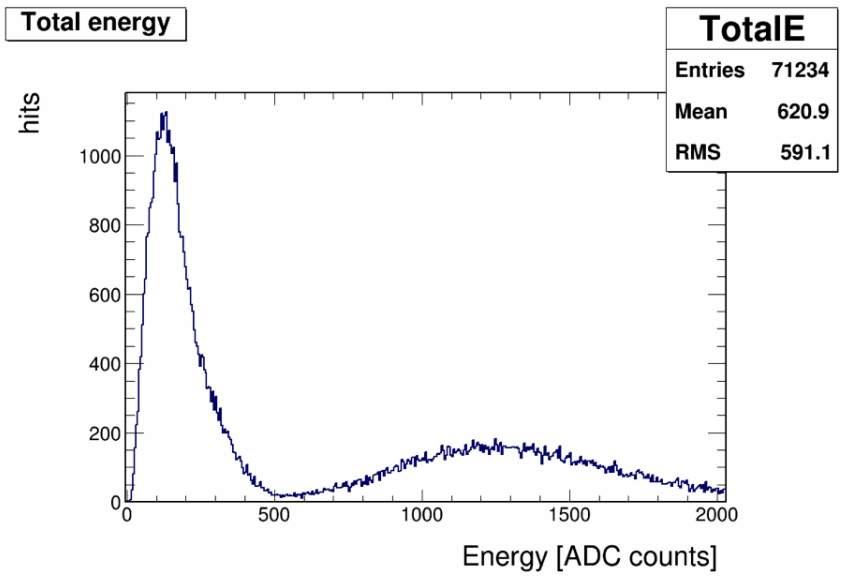

Figure 14: Energy deposition for a $(e^- + \mu)$ beam.

identified as coming from the muons in the beam and is well separated from the wide distribution of the electrons. Using events with ADC counts above 550 assures to separate the electron events.

5.2 Signal processing

The basic steps of signal processing, used for each event, included the following [12]:

- base-line removal and RMS calculation for each channel (samples 0 - 14);
- common-mode subtraction;
- deconvolution filter of CR-RC shape (sampling period of 50 ns and shaping time of 68 ns).

Figure 15 shows the raw signal of an electron event in each of the four planes. After processing

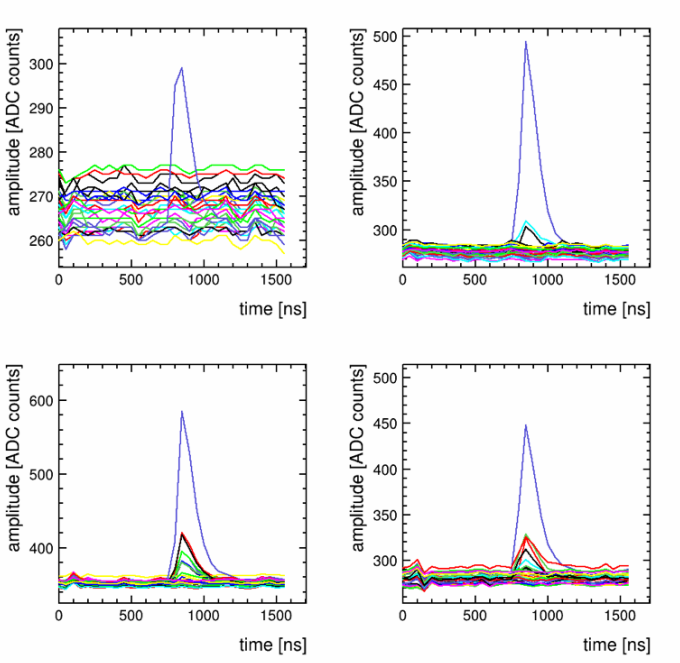

Figure 15: The profile of the 32 sampling of one electron event using the raw data signal in plane 1 (upper left), plane 2 (upper right), plane 3 (lower left) and plane 4 (lower right).

through the steps mentioned above, the signals in the four planes of the same electron event are sown in Figure 16.

5.3 Electromagnetic shower

In order to analyze the longitudinal development of the electromagnetic shower, the energy deposited in each sensor plane for each configuration was used. Distribution of the energy sum per layer in a single event, for each of the three configurations, is shown in Figure 17. The top four figures show this distribution for the first configuration in which the first sensor layer was after one absorber (see Figure 4). The four figures in the second row present the energy sum distribution per layer in the second configuration where the first sensor layer was placed after three absorber layers. The last row shows the distribution for the configuration where the first layer was put after four absorber layers. As slready mentioned above, the reason that there are only results from three layers is because in this configuration the fourth sensor was malfunctioning (see also Table 1).

The longitudinal development of electron showers is shown in Figure 18 in terms of average shower energy deposits per plane as a function of the number of absorber layers. All plane configurations are represented in the plot. The uncertainties shown on the data are mainly systematic

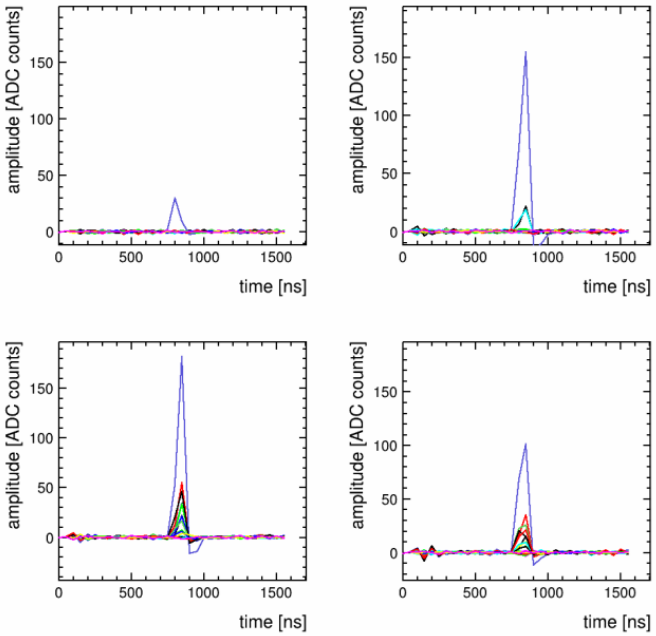

Figure 16: The profile of the 32 sampling of the same electron event as shown in Figure 15, after processing the signal in plane 1 (upper left), plane 2 (upper right), plane 3 (lower left) and plane 4 (lower right).

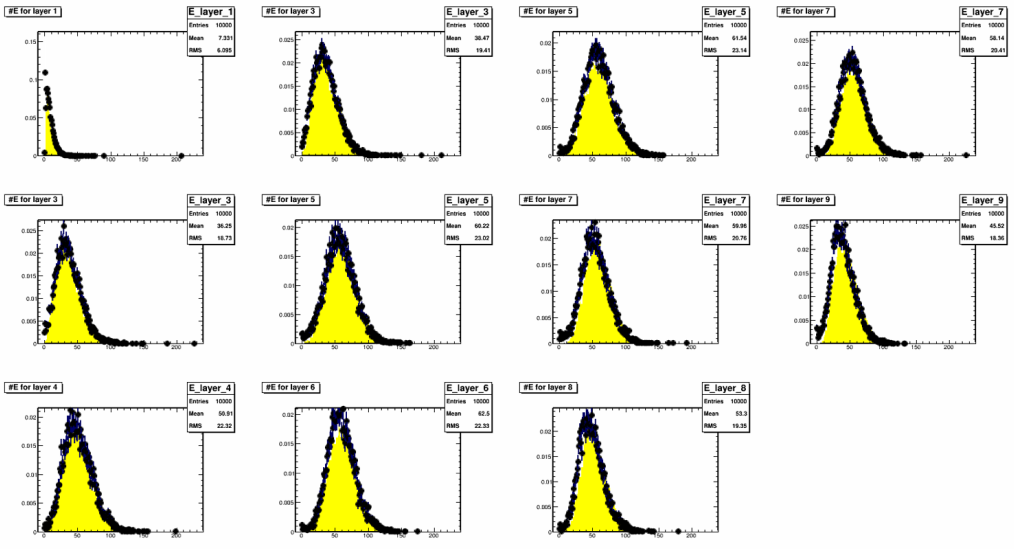

Figure 17: Distribution of the energy sum per layer in a single event, for each of the three configurations (see Table 1). The top four figures show the energy distributions of the first configuration, the middle four - that of the second configuration and the last three present energy distributions in configuration three.

uncertainties coming from the calibration of a MIP signal for each layer. This uncertainty was

estimated to be about 5%.

The measurement results were compared with prediction of GEANT4 [13] Monte Carlo simulations where the experimental setup was implemented. As can be seen, good agreement was found between them. The shower maximum is observed after 6 radiation lengths.

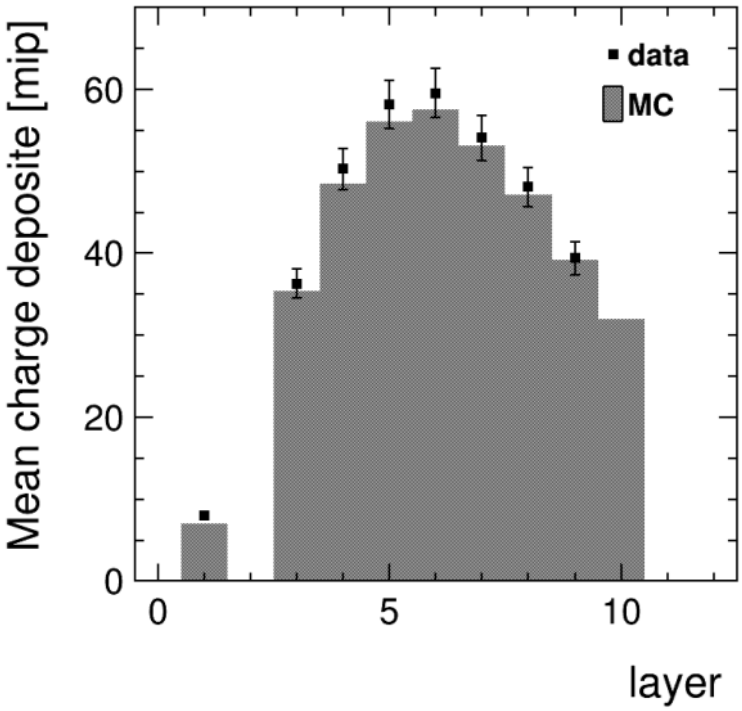

Figure 18: Average energy deposited in the instrumented area of the LumiCal detector prototype as a function of the number of tungsten absorber layers (approximately equal to radiation length). The dots are the data and the shaded area, the MC simulation.

6. Conclusions and outlook

We carried out for the first time a multi-plane operation of a prototype of a luminometer designed for a future e^+e^- collider detector. The test was performed successfully in the CERN PS accelerator T9 testbeam. We studied the development of the electromagnetic shower and described the results with a GEANT4 Monte Carlo simulation.

In the next stage of the test data analysis we plan to determine the Moliere radius, compare hadron, muon and electron runs, apply clustering and reconstruct showers for spatial and angular resolutions.

Acknowledgments

We would like to thank all our colleagues from the FCAL collaboration who helped with the preparation and operation of this test beam. This study was partly supported by the Israel Science Foun-

dation (ISF), Israel German Foundation (GIF), I-CORE, the Rumanian UEFISCDI agency, by the Ministry of Education, Science and Technological Development of the Republic of Serbia, and by the EU H2020 project AIDA-2020.

References

[1] H. Abramowicz et al., [FCAL Collaboration], *Forward Instrumentation for ILC Detectors*, JINST **5** (2010) 12002.

[2] Ch. Grah and A. Sapronov, *Beam parameter determination using beamstrahlung photons and incoherent pairs*, JINST **3** (2008) 10004.

[3] P. Bambade, V. Drugakov and W. Lohmann, *The Impact of BeamCal performance at different ILC beam parameters and crossing angles on tau searches,* Pramana **69** (2007) 1123.

[4] H. Abramowicz et a;., [FCAL Collaboration], *Performance of fully instrumented detector planes of the forward calorimeter of a Linear Collider detector,* JINST **10** (2015) P05009.

[5] F.-X. Nuiry, *Collected documents on the FCAL-AIDA precision mechanical infrastructure and tungsten plates.* https://edms.cern.ch/document/1475879/.

[6] J. Baudot et al., *First test results of MIMOSA-26: A fast CMOS sensor with integrated zero suppression and digitized output,* http://inspirehep.net/record/842163?ln=en.

[7] D. Cussans, *A Trigger/Timing Logic Unit for ILC Test-beams,* Proceedings of the Topical Workshop on Electronics for Particle Physics, TWEPP-07, Prague, Czech Republic, 3-7 September 2007. http://indico.cern.ch/event/11994/session/29/contribution/11/attachments/63972/91915/cussans_d_twepp2007_proceedings.pdf;
D. Cussans, *Description of the JRA1 Trigger Logic Unit (TLU),* EUDET-Memo-2009-4 https://www.eudet.org/e26/e28/e42441/e57298/EUDET-MEMO-2009-04.pdf.

[8] J. Baudot, *TAF short manual,* http://www.iphc.cnrs.fr/IMG/pdf/taf_shortdoc.pdf, http://www.iphc.cnrs.fr/TAF.html.

[9] S. Kulis, *Development of prototype luminosity detector modules for future experiments on linear colliders.* PhD thesis, AGH - UST, Cracow, Dec 2012, CERN-THESIS-2012-358.

[10] L. Rossi, *Pixel detectors: from fundamental to applications,* Particle acceleration and detection, Springer 2006.

[11] T. Preda, *A method for muon-electron discrimination in the LumiCal test beam,* https://agenda.linearcollider.org/event/ 6846/contribution/3/material/slides/.

[12] J. Moron, *Development of novel low-power, submicron CMOS technology based, readout system for luminosity detector in future linear collider,* Ph. D. dissertation, AGH - UST, Cracow, July 2015.

[13] S. Agostinelli et al., *GEANT4 - a simulation toolkit,* Nucl. Inst. Meth. **A 506** (2003) 250.